NANO LETTERS

2002
Vol. 2, No. 3
245−252

Crystallite Size Variations of Nanosized Fe_2O_3 Powders during γ- to α-Phase Transformation

Fu Su Yen,* Wei Chien Chen, Janne Min Yang, and Chen Tsung Hong

Department of Resources Engineering, National Cheng Kung University, Tainan, Taiwan 70101, ROC

Received November 16, 2001

ABSTRACT

Crystallite size variations of nanosized iron oxide particles during γ- to α-phase transformation were examined using DTA/TG, FTIR, XRD, TEM, and BET-N_2 techniques. Synthetic γ-FeOOH and Fe_3O_4, prepared as precursors, both converted to γ-Fe_2O_3 and then completed the phase transformation under thermal treatment. Starting with γ-FeOOH, the γ-Fe_2O_3 obtained grew from the original size of 5 nm to a size about 25 nm or larger, then transformed to α-Fe_2O_3. The α-crystallites obtained showed sizes similar to that of γ-crystallite. With continuous heating, the α-Fe_2O_3 coarsened to a size of ~55 nm. Identical phenomena were observed when α-Fe_2O_3 was prepared from Fe_3O_4 via γ-Fe_2O_3. The study also found that α-Fe_2O_3 crystallites obtained by calcinations of amorphous $Fe(OH)_3$ will show sizes smaller than 5 nm. The decomposition temperature can be lowered to 200 °C.

1. Introduction. Size-induced structural phase transformation of γ- to α-Fe_2O_3 has been reported previously.[1,2] Observations on samples with narrow size distributions and different mean sizes of iron oxide show that γ- to α-Fe_2O_3 phase transformation occurs beginning with sizes of 30 nm. Above that size, the stable phase is α-Fe_2O_3 (rhombohedral, corundum structure), while below that size the stable phase is found to be γ-Fe_2O_3 (cubic, spinel structure). Recent studies[3−5] on the boehmite-derived nanosized alumina (Al_2O_3) powders (dia.<100 nm, XRD-Scherrer formula[6] on $(012)_\alpha$) reveal that the phase transformation from θ- to α-Al_2O_3 shows similar phenomena. There are critical sizes for θ- and α-Al_2O_3 crystallites during phase transformation, and transformation occurs once the θ-crystallites have grown to a size approaching 25 nm during the heat treatment, at which point one θ-crystallite can form one α-crystallite. In addition, α-Al_2O_3 crystallites show a critical size of 17 nm for nucleation. However, with continuous heating, the nucleus grows to a size of 45−50 nm, which is considered as the primary crystallite size by the coalescence of the nuclei. At that point the phase transformation is accomplished.

The isostructural relationships between iron and aluminum compounds are well known.[7] For example, lepidocrocite (γ-FeO(OH)) is isotructural to boehmite (AlO(OH)), geothite (α-FeO(OH)) is so to diaspore, and hematite (α-Al_2O_3) is so to corundum (α-Al_2O_3). In addition, there can be similar phenomena of critical and primary sizes during γ- to α-Fe_2O_3 phase transformation. An understanding of these size phenomena can be helpful to the manufacturing of the nanosized iron oxide powders, which is more an increasing important part of ferrite technology because of the greater miniaturization of devices.

In this study, crystallite size variations of γ- and α-Fe_2O_3 during phase transformation are examined using two γ-Fe_2O_3 powders obtained by calcinations of synthetic Fe_3O_4 (magnetite) and γ-FeO(OH) (lepidocrocite), respectively. Discussion focuses on the thermal behavior of the transformation process examined by differential thermal analysis (DTA), in relation to both the crystallite size variations of γ- and α-Fe_2O_3 and the quantity of α-Fe_2O_3 formation.

2. Experimental Section. *2.1. Precursor Preparation.* 2.1.1. Preparation of γ-FeO(OH). Reagent grade ferric chloride ($FeCl_2 \cdot 4H_2O$, EP, Merck), hexamethylenetetramine ($(CH_2)_6N_2$, EP, Merck), and sodium nitrate ($NaNO_3$, EP, Merck) were used as the starting materials.[8] First, 16 g of $FeCl_2 \cdot 4H_2O$, 22.4 g of $(CH_2)_6N_2$, and 5.6 g of $NaNO_3$ were dissolved in 400, 80, and 80 mL of DI water, respectively, to form three solutions. Then a homogeneous mixture for the three solutions was followed to obtain a bluish green precipitate. The precipitate remained in the solution (pH = 6.0 ~6.4, in the original container) and was aged at 60 °C for 3 h. The product was centrifuged to separate the precipitate. The precipitate was washed three times with distilled water and finally once with ethyl alcohol to remove anions and organic impurities and then vacuum-oven dried at 60 °C for 48 h. The dried gel was ground to −200 mesh

* Corresponding author. E-mail: yfs42041@mail.ncku.edu.tw. Phone: +886-6-2355603. Fax: +886-6-2380421.

10.1021/nl010089m CCC: $22.00
Published on Web 01/10/2002

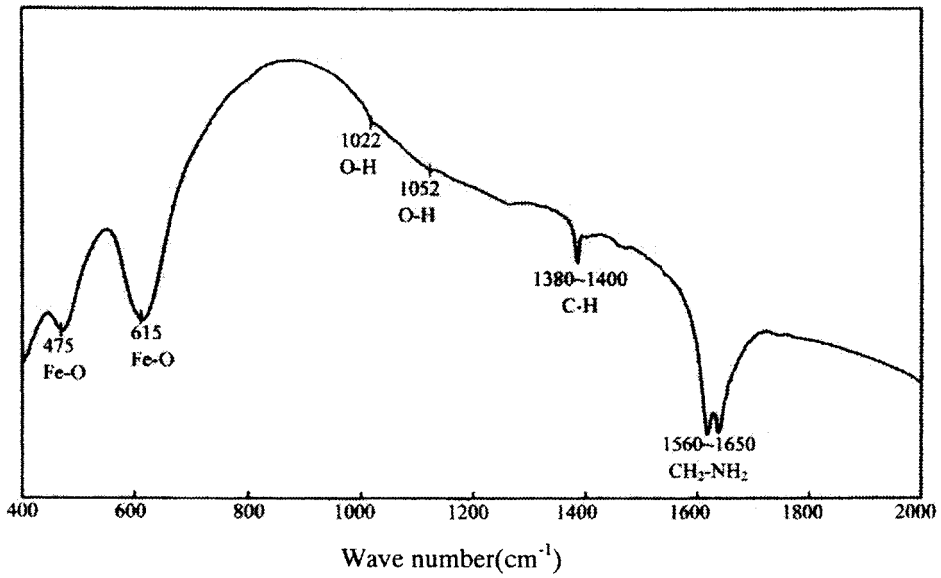

Figure 1. Infrared spectra of γ-FeO(OH) xerogels.

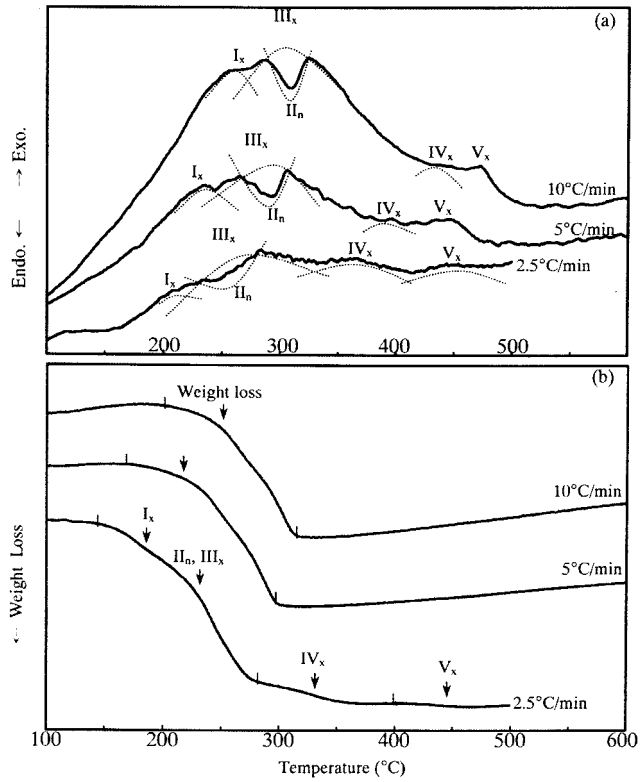

Figure 2. (a) Differential thermal analysis (DTA) and (b) corresponding thermogravimetric analysis (TG) profiles of γ-FeO(OH) xerogels with heating rates of 2, 5, and 10 °C/min.

(<74 μm). A deep orange-colored γ-FeOOH powder was obtained. FTIR spectral examination revealed that the powder was γ-FeOOH[9] with a detectable presence of organic impurities (Figure 1). Additional phase identification using XRD techniques also showed that, in additino to lepidocrocite, it contained a small amount of magnetite (Fe_3O_4) (Figure 3a). The powder then was used as a starting material for this study.

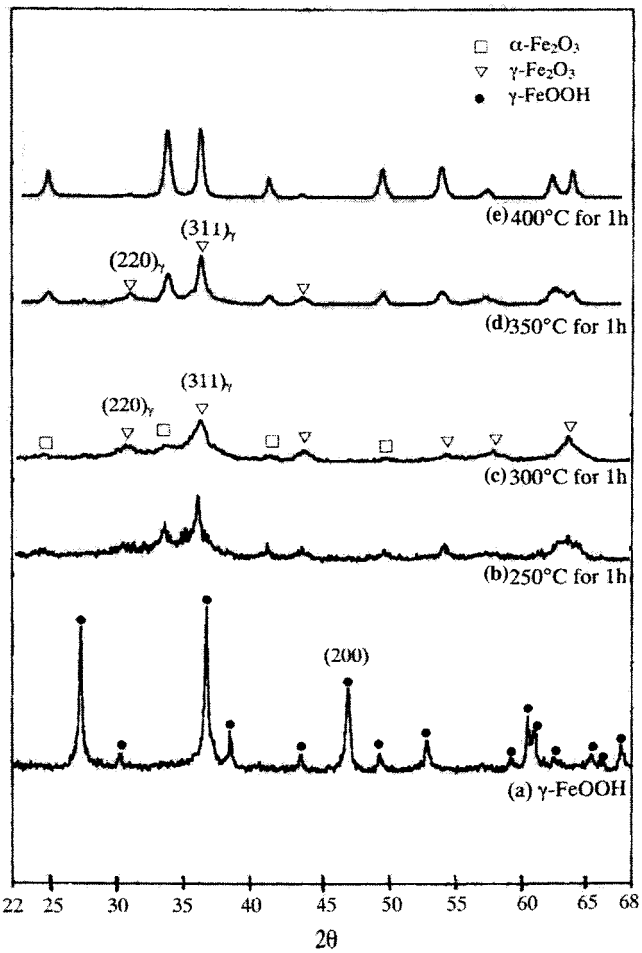

Figure 3. XRD patterns of calcined γ-FeO(OH) xerogel powders: (a) as prepared; and calcined at (b) 250 °C, (c) 300 °C, (d) 350 °C, and (e) 400 °C for 1 h. The heating rate was 5 °C/min.

2.1.2. Pure Iron-Containing Tartrate Gel. Tartrate gel techniques[10,11] were employed to synthesize magnetite (Fe_3O_4)

using reagent grade chemicals. Ferric nitrate ($Fe(NO_3)_3 \cdot 9H_2O$, EP, Katayama) and tartaric acid ($C_2H_2(OH)_2(COOH)_2$, EP, Katayama) were dissolved in and then adjusted separately with ethyl alcohol (99.5%, Seoul) to form two solutions of Fe^{3+} (0.2 mol/L) and tartaric acid (0.24 mol/L). Tartrate precipitates were then obtained by titrating one volume unit of solution Fe^{3+} into one volume unit of stirred tartaric acid solution. It should be noted that the tartaric acid used for titration was 20% in excess over the stoichiometric amount needed to meet the charge balance. The precipitates remained in solution in the original container for 1 h with constant stirring to ensure that the reaction was complete. Then it was vacuum oven dried for 24 h. The dried gel was ground to −200 mesh (<74 μm) and used as another starting material for this study.

2.2. Calcined Powders. A preliminary test for the two starting powders using differential thermal analysis/thermogravimetric analysis (DTA/TG), compared with phase analysis using X-ray diffraction (XRD), was made to evaluate the necessary temperature and process for calcination of the gel powder. Additionally, pretreatments for the gel powder at temperatures between 200 and 300 °C for various times were made to remove the volatile organic compounds and prepare the γ-Fe_2O_3 powders.

2.2.1. Powder Characterization. Thermal behavior examinations of both the xerogel powder and the preheat-treated powder were conducted using DTA/TG techniques (Setaram TGA92) in air at a heating rate of 5 °C/min, and 2 and 10 °C/min, as necessary. The reference sample was well crystallized α-Al_2O_3 powder. The crystalline phase identification for the calcined powders was performed by XRD powder methods using Ni-filtered CuKα radiation, 30 kV × 20 mA (Rigaku, Tokyo). XRD powder methods were also employed to determine α-Fe_2O_3 formation using CaF_2 as the internal standard. The calibration line was established by calculating area ratios between α-Fe_2O_3 (104) and CaF_2 (111) measured from a series of γ-Fe_2O_3 samples in which varying ratios of α-Fe_2O_3 and 10 wt % CaF_2 were formulated.

The mean crystallite sizes of magnetite (Fe_3O_4) and γ- and α-Fe_2O_3 of the powders were determined by the XRD-Scherrer formula (mean crystallite size $= 0.9\lambda/(B \cos \theta)$, where $\lambda = 1.540562$ Å, $B =$ broadening of width at the half-peak height (WHPH) in radian, and $\theta =$ Bragg angle)[6]. It was applied to peaks of (220), (104), and (220) of magnetite, α -, and γ-Fe_2O_3, respectively, with a scanning rate 0.5°/min. The instrument peak width calibration was obtained using a well-crystallized silicon powder. The calculation was assisted by a software, XRD Pattern Processing and Identification, Jade for Windows, Version 3.0 developed by Material Data Inc. The conventional nitrogen absorption technique (BET-N_2) (Micromeritics, Gemini 2360) was adopted to measure the specific surface area of the observed samples, by which the surface area diameter of the sample was evaluated.

Transmission electron microscopic techniques (TEM, JEOL, AEM-3010) were employed to examine the morphology and the microstructure of particles present in the transformation systems.

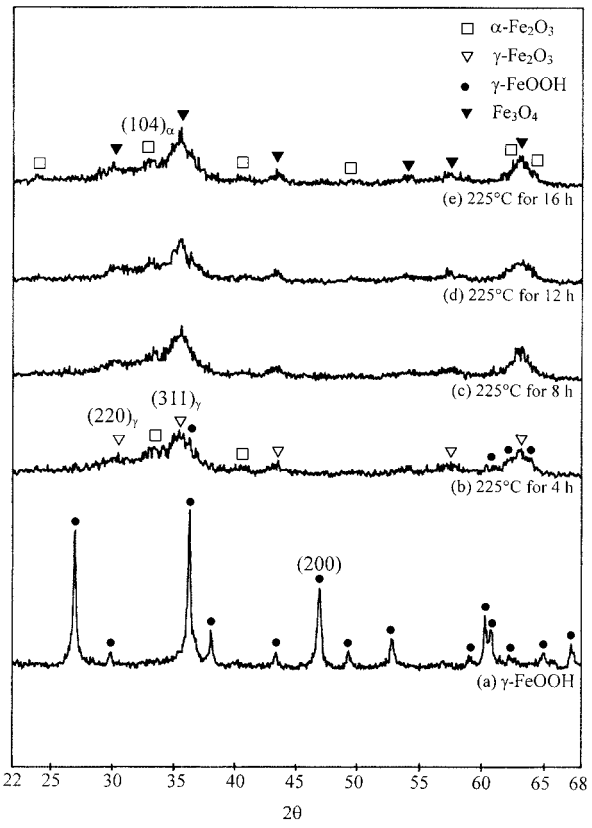

Figure 4. XRD patterns of γ-Fe_2O_3 powders prepared by calcination of γ-FeO(OH) xerogels at 225 °C for varying times. Sample (d) was selected for further examination.

3. Results and Discussion. *3.1. Thermal behavior of γ-FeOOH.* Figure 2 displays DTA/TG curves of γ-FeOOH xerogel powders measured by heating rates of 2, 5, and 10 °C/min. The corresponding XRD patterns are shown in Figure 3. Four exothermic reactions, Ix, IIIx, IVx, and Vx, and one endothermic reaction, IIn occurred. The exotherm Ix resulted from the thermal decomposition of the organic matter. The endotherm IIn that corresponds to the decomposition of γ-FeOOH[12] is followed by the formation of γ-Fe_2O_3, IIIx (Figure 3b). There is a small amount of magnetite transformed to γ-Fe_2O_3 at IVx (Figure 3d), which brought a substantial increase in weight (IVx on TG curve of 2.5 °C/min heating rate). The main phase transformation of γ- to α-Fe_2O_3 took place at Vx. (Figure 3e).

It is noted that, as the heating rate increased, the weight gain on TG curves changed. The oxidation of Fe_3O_4 to γ-Fe_2O_3 persisted to temperatures above 600 °C, indicating that a slower heating rate may favor the oxidation reaction. Thus it is clear that if one wishes to obtain γ-Fe_2O_3 by calcination of the γ-FeOOH gel, annealing at lower temperature must be employed. The examination of γ- to α-Fe_2O_3 phase transformation was then carried out using γ-Fe_2O_3 powders instead of direct use of γ-FeOOH xerogel. Figure 4 illustrates the XRD profiles of γ-Fe_2O_3 powders obtained by calcination of γ-FeOOH gels at 225 °C for various times. Clearly, there were traces of Fe_3O_4 and α-Fe_2O_3 phases and substantial amounts of amorphous phases (designed as $Fe(OH)_3$) present in the powders. Comparing the amount of trace mineral phases, it was decided to adopt

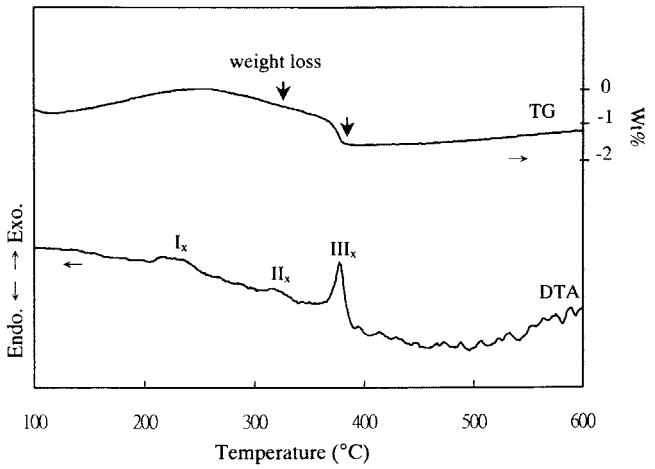

Figure 5. Typical DTA and TGA profiles of γ-Fe_2O_3 powders with a heating rate of 5 °C/min.

the sample of 12 h annealing time for further examination. The γ-Fe_2O_3 powder contains detectable amounts of Fe_3O_4, α-Fe_2O_3, and amorphous "$Fe(OH)_3$". The mean crystallite sizes of γ- and α-Fe_2O_3 (XRD-Scherrer formula, (220) γ and (104) α) in the prepared γ-Fe_2O_3 powder were 4.5 and 2.5 nm, respectively. The BET-N_2 (surface area) diameter of the powder system was 11 nm.

3.2. Crystallite Sizes of γ- and α-Fe_2O_3. 3.2.1. γ-Fe_2O_3 powder derived from γ-FeOOH. Figure 5 displays DTA/TG curves of the γ-Fe_2O_3 powder obtained by calcination of the γ-FeOOH xerogel powder used in this study. The heating rate was 5 °C/min. The corresponding XRD patterns are shown in Figure 6. The exotherm Ix (250 °C) resulted from the oxidation of Fe_3O_4 to γ-Fe_2O_3, which brought an increase in weight. The exotherm IIx occurred at temperature ~325 °C and was the dehydration of $Fe(OH)_3$ to form α-Fe_2O_3[9]. At temperature ~400 °C, IIIx, abundant α-Fe_2O_3 was transformed from γ-Fe_2O_3.

Figure 7 demonstrates the relationships between the amount of α-Fe_2O_3 formation, the crystallite sizes of γ- and α-Fe_2O_3, and BET-N_2 diameter during γ- to α-phase transformation of the γ-Fe_2O_3 powder system. The observed samples were heated to the anticipated temperatures with a heating rate identical to that used in Figure 6, then quenched to room temperature to freeze the phase transformation process at specific temperatures. In general, the temperature at which the increase in α-Fe_2O_3 formation occurred was consistent with that observed on DTA profile. And the growth of γ- and α-Fe_2O_3 crystallite (mean) sizes indicates that they can be transformed from $Fe(OH)_3$, Fe_3O_4, and mainly from γ-Fe_2O_3 crystallites at the temperatures corresponding to the exotherms shown on DTA profile. The crystallite size of γ-Fe_2O_3 remained between 4 and 7 nm in the temperature range of 250 to 350 °C (Figure 10a), while the size of α -crystallites was 2.5~3.0 nm, which was the original α -size existing in the γ-Fe_2O_3 powder. As the temperature increased, the α-size coarsened to a size of 5 nm. Then it decreased slightly as exotherm IIx occurred, indicating that α-Fe_2O_3 derived from $Fe(OH)_3$ showed sizes smaller than 5 nm. Clearly, the dehydration and the formation

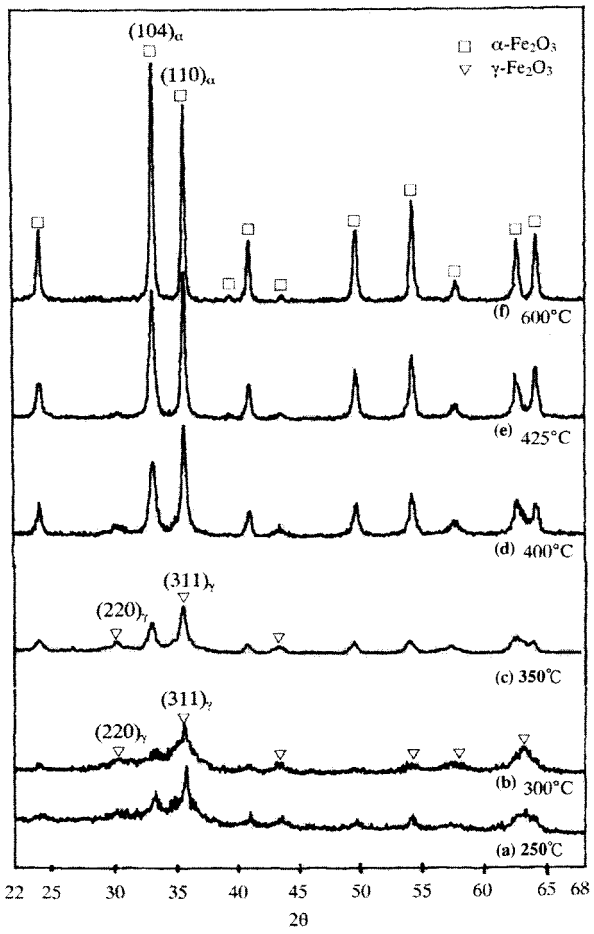

Figure 6. XRD patterns of calcined γ-Fe_2O_3 powders with a heating rate of 5 °C/min, then quenched to room temperature.

of α-Fe_2O_3 from $Fe(OH)_3$ may be initiated at temperatures as low as 200 °C and prolonged until ~400 °C (Figure 7). The highest yield of the α-Fe_2O_3 crystallite from $Fe(OH)_3$ occurred at IIx, resulting in a size reduction of the α-Fe_2O_3 crystallites. However, it is noted that, within the temperature range, the quantity of α-Fe_2O_3 formation of the powder system is less than 15 wt %. By the time the temperature of IIIx occurred, both the crystallite sizes of γ-and α-Fe_2O_3 and the quantity of α-Fe_2O_3 formation increased rapidly, and the γ-size coarsened from 8~12 to 25 nm. Meanwhile, α-sizes increased from 5, 10, 20, then to 25 nm. And the amount of α-Fe_2O_3 present increased from 15% to ~90%. The fast and smooth increase in α -sizes presumably reveals that there was a rapid appearance of α -crystallites with sizes about 25 nm, bringing about an increase of the mean α -crystallite size to the powder system. As phase transformation progresses, α-crystallites may appear with sizes close to that of γ-crystallite. These phenomena simply imply that γ-Fe_2O_3 derived from both Fe_3O_4 and γ-FeOOH may need to grow to a size of ~25 nm before the phase transformation of γ- to α-Fe_2O_3 takes place. Thus there can be critical sizes of phase transformation for γ- and α-Fe_2O_3, although the crystallite size may be smaller than the previously reported 30 nm[2]. Furthermore, the transformation is based on one γ -crystallite to one α-crystallite. Similar phenomena were observed during θ- to α-Al_2O_3 phase transformation.[3−5] The α-Fe_2O_3 crys-

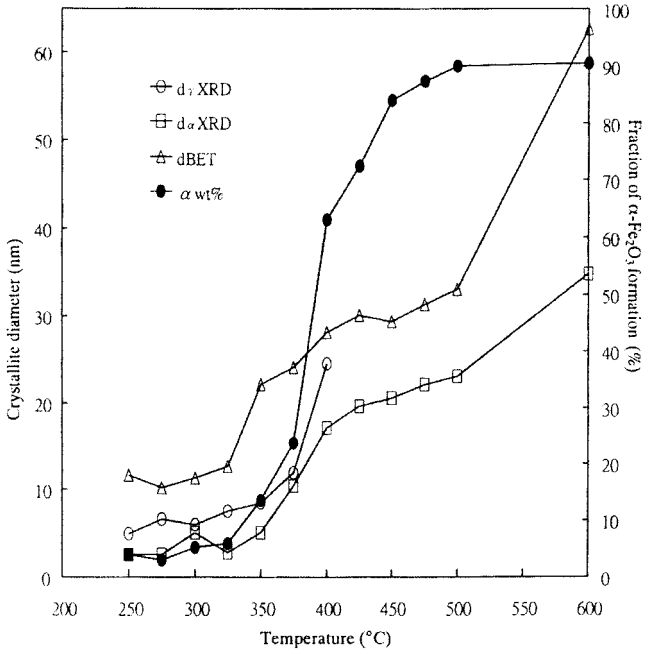

Figure 7. Relationships among the amount of α-Fe_2O_3 formation, γ- and α-Fe_2O_3 crystallite sizes, and BET-N_2 diameter during γ- to α-phase transformation of γ-Fe_2O_3 powder system.

tallite then coarsened to a size of about 55 nm by coalescence of the α-Fe_2O_3 crystallites of ∼25 nm size, since the amount of α-Fe_2O_3 formation remained 90%. At 600 °C, polycrystallite particles occurred (refer to BET diameter and α-size in Figure 7). It is noted the α-Fe_2O_3 formation reached only 90%. This may be attributed to the transformation of a substantial amount of Fe_3O_4 into γ-Fe_2O_3 (Figure 2, heating rates 5 and 10 °C/min) that cannot reach the critical size of phase transformation at the late stage of γ- to α-Fe_2O_3 phase transformation, similar to the situation occurs in the case of θ- to α-Al_2O_3 phase transformation.[5] However, it is not currently clear if the 55 nm size is the primary size of phase transformation.

3.2.2. γ-Fe_2O_3 Derived from Fe_3O_4. Additional proof using magnetite as the starting material to demonstrate the critical size phenomena was examined. To attain samples for observing the transformation process, thermal treatments with a heating rate of 5 °C/min through the quench technique were conducted to prepare samples from Fe_3O_4. Figure 8 shows the relationships between the α-Fe_2O_3 phase formation and the size variations of γ- and α-Fe_2O_3 crystallites and BET diameter of the calcined Fe_3O_4 powders during γ- to α-Fe_2O_3 phase transformation. The DTA profile with identical heating rate of the magnetite powder system was also inserted. The corresponding XRD patterns used for phase identification are shown in Figure 9.

The thermal decomposition of Fe-tartrate has been discussed previously.[9] Magnetite is formed at temperatures about 250 °C, transforming to γ-Fe_2O_3 through oxidation at temperatures around 300 °C. Then γ- to α-Fe_2O_3 phase transformation occurs at 425 °C (Figures 8 and 9). The mean crystallite size of Fe_3O_4 (Scherrer formula-XRD, (220)) at temperature 300 °C was 15 nm. The crystallite size of γ-Fe_2O_3 (Scherrer formula-XRD, (220)) obtained by oxidation of Fe_3O_4 crystallites was similar to that of the magnetite. The size remained unchanged as well as that shown by the BET-N_2 diameter of the powder system (17.5 nm), indicating that both the particle size and the crystallite size of the powder system remained unchanged during the magnetite to γ-Fe_2O_3 transformation. Then it was found that, at 400 °C, blooming of α-Fe_2O_3 formation started with crystallite size ∼25 nm (Figure 8). The final γ-crystallite size observed at that stage was ∼24 nm (450 °C). The α-Fe_2O_3 crystallite, although it coarsened slightly, persisted in the same size, ∼30 nm, during the blooming of the α-Fe_2O_3 formation until the end of the phase transformation (∼525 °C, >97% of α-Fe_2O_3 formation in Figure 8). The size relationship demonstrates that the α-crystallite obtained from phase transformation of γ-Fe_2O_3 crystallites is carried out once the

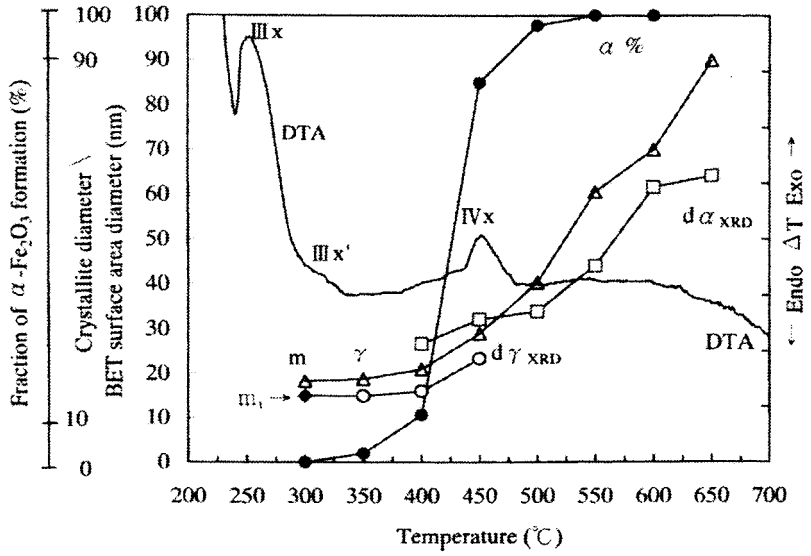

Figure 8. Relationships between the amount of α-Fe_2O_3 formation, γ- and α-Fe_2O_3 crystallite sizes, and BET-N_2 diameter during γ- to α-phase transformation of Fe_3O_4 powders derived from Fe-tartrate. (α-Fe_2O_3 formation, ●; crystallite size of α-Fe_2O_3, □; γ- Fe_2O_3, ○; magnetite, ◆; BET-N_2 diameter, △. DTA profile is inserted.

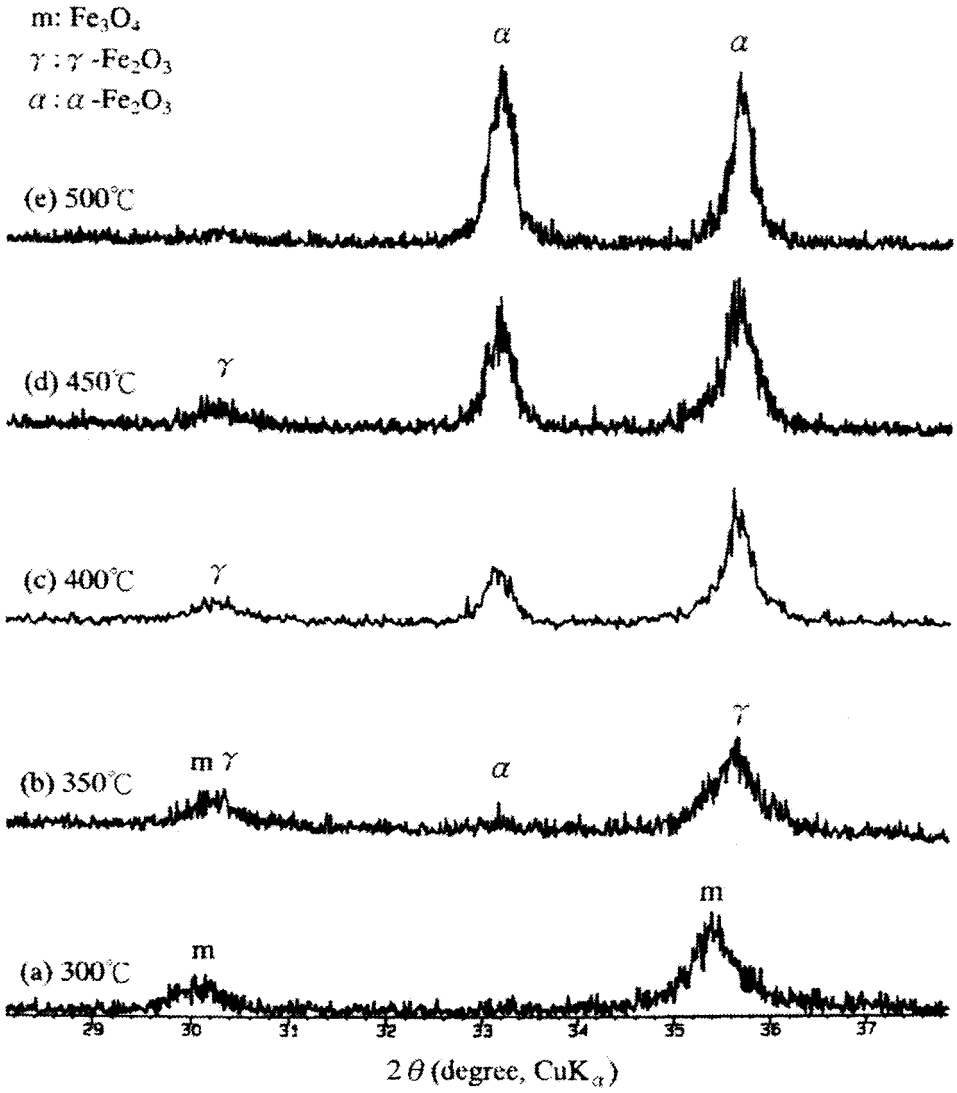

Figure 9. XRD patterns of Fe-tartrate heated to temperatures (a) 300 °C, (b) 350 °C, (c) 400 °C, (d) 450 °C, and (e) 500 °C, and then quenched to room temperature. The heating rate was 5 °C/min.

γ-Fe_2O_3 grows to a size about 25 nm. The transformation is a one γ- to one α-crystallite transformation.

It should be noted that the BET-N_2 diameter was clearly increasing as the γ-size increased. However, the diameter remained between the sizes of γ- and α-Fe_2O_3, and was smaller than that of α-Fe_2O_3, because the mean crystallite size of α-Fe_2O_3 eventually was only composed of crystallites with sizes equivalent to or larger than 25 nm. However, with continuous heating, the BET-N_2 diameter increased and eventually exceeded α-sizes at the end of phase transformation, indicating that polycrystallite α-Fe_2O_3 particles were forming. Apparently, the appearance of polycrystallite α-particles initiated the formation of α-Fe_2O_3 crystallites with sizes ~60 nm when the phase transformation approached 100%. And thus the appearance of α-Fe_2O_3 with crystallite size ~60 nm is apparently achieved by the coalescence of the 25 nm-sized α-Fe_2O_3 crystallites (dα at 600 and 650 °C in Figure 7).

Thus magnetite crystallites derived both from γ-FeOOH and tartrate gels converted to γ-Fe_2O_3, and then transformed to α-Fe_2O_3 by similar critical sizes. This is as expected, since the crystallite size of the magnetite derived from tartrate was coarser, it could transform to γ-Fe_2O_3 at higher temperatures, compared with magnetite from γ-FeOOH. However, comparing the peak temperatures IIIx (375 °C) and IVx (450 °C) on DTA profiles in Figures 5 and 7, respectively, temperature may not be the controlling factor for γ- to α-Fe_2O_3 phase transformation. And the smaller α-crystallite size observed in Figure 5, compared with that in Figure 7, during the blooming of α-crystallite formation can be attributed to the presence of α-crystallite derived from $Fe(OH)_3$. It is noteworthy that α-Fe_2O_3 will show crystallite sizes less than 5 nm if it is derived from $Fe(OH)_3$. Additionally, further examination is necessary to determine whether α-Fe_2O_3 crystallites will grow to a size of 55 to 60 nm, as the primary crystallite, before the transformation is accomplished.

3.3. Micrographs of α-Fe_2O_3 Crystallites. Typical TEM micrographs of γ- and α-Fe_2O_3 crystallites are shown in Figure 10. It is noted that α-Fe_2O_3 crystallites obtained by calcination of γ-Fe_2O_3 derived from γ-FeOOH, due to the presence of amorphous $Fe(OH)_3$, eventually show sizes

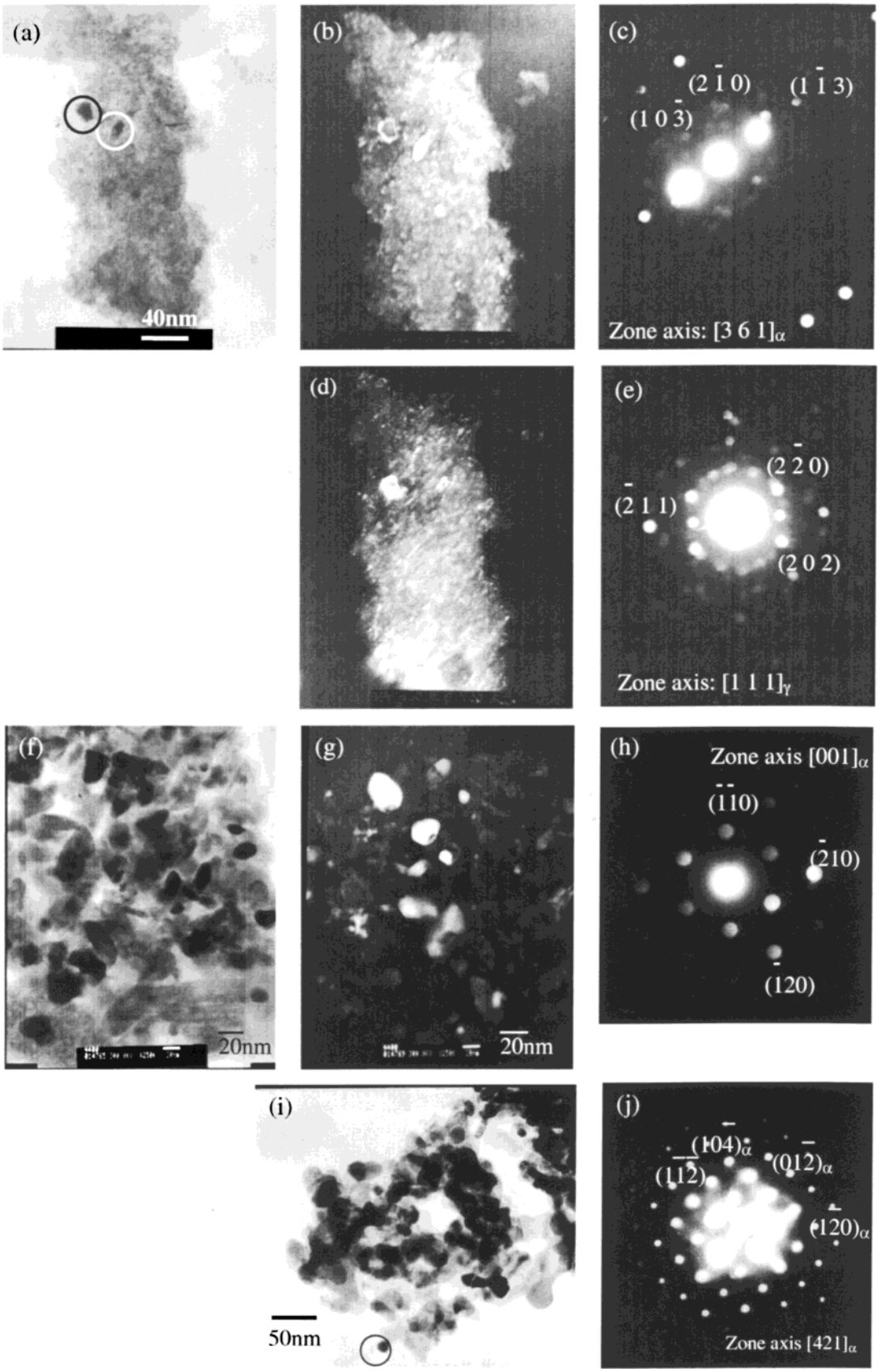

Figure 10. Typical TEM micrographs of γ- and α-Fe_2O_3 crystallites. (a−c): α-Fe_2O_3 obtained by dehydration of "$Fe(OH)_3$ " in γ-FeO-(OH) gels, (250 °C for 1h). Image (b) is the dark field image of white circle regions in (a) with corresponding electron diffraction (ED) pattern shown as (c). (d−e): γ-Fe_2O_3 transformed from Fe_3O_4 (γ-FeO(OH) calcined at 250 °C for 1h). Image (d) is the dark field image of black circle regions in (a) with corresponding ED pattern shown as (e). (f−h): Three sizes of α-Fe_2O_3 crystallites observed in the α-Fe_2O_3 powders obtained by heating γ-Fe_2O_3 to 400 °C, and then quenched. (i, j): α-Fe_2O_3 powders with crystallite size ~25 nm (450 °C quenched sample).

smaller than 5 nm (Figure 10a, b, and c) as well as with γ-Fe_2O_3 crystallites of sizes ~5 nm (Figure 10d and e). The latter grow to the size of ~25 nm, then transform to α-Fe_2O_3 (Figure 7). Thus α-crystallites derived from γ-Fe_2O_3 of γ-FeOOH origin will show α-Fe_2O_3 crystallites with three different sizes (Figure 10f, g, and h). α-Crystallites derived from γ-Fe_2O_3 of magnetite origin may show crystallite of mono size, ~25 nm, during the transformation, before the α-Fe_2O_3 grows to the size of ~55 nm (Figure 10i and j).

4. Conclusion. In this study, crystallite size variations during γ- to α-phase transformation of nanosized Fe_2O_3 powders were examined. Samples of γ-Fe_2O_3 derived from both synthetic γ-FeOOH and Fe_3O_4 powders were used to prepare γ-Fe_2O_3, from which the nanosized α-Fe_2O_3 powder was obtained.

Starting with γ-FeOOH, the γ-Fe_2O_3 obtained grew from a size of 5 up to 25 nm or larger, and then transformed to α-Fe_2O_3. However, γ-Fe_2O_3 crystallites derived from Fe_3O_4 showed sizes larger than 15 nm, behaved similarly, grew to the size of 25 nm, and then transformed to α-Fe_2O_3. The α-crystallites thus obtained had sizes about 25 nm. Consequently, there can be a critical size of phase transformation for γ- to α-Fe_2O_3 crystallites. With continuous heating, the 25-nm α-crystallites would coarsen to a size of 55 to 60 nm.

α-Fe_2O_3 crystallites obtained by calcinations of amorphous $Fe(OH)_3$ will show sizes less than 5 nm. The decomposition temperature of $Fe(OH)_3$ can be lower than 200 °C.

Acknowledgment. The authors wish to express their grateful acknowledgment to professors T. T. Ray and M. H. Tsai of National Cheng Kung University for their valuable discussion. The authors also wish to express their gratitude to Miss L. Z. Wang of National Sun yet San University for assistance in TEM photography. This study was financially supported by the National Science Foundation of the Republic of China under Contract No. 89-2216-E006-086.

References

(1) Mulaani, M. S.; Ayyub, P. *Condens. Matter News* **1991**, *1*(1) 25.
(2) Ayyub, P.; Multani, M.; Barma, M.; Palkar, V. R.; Vijayaraghavan, R. *J. Phys. C: Solid State Phys.* **1988**, *21*, 2229.
(3) Wen, H. L.; Chen, Y. Y.; Yen, F. S.; Huang, C. Y. *Nanostruct. Mater.* **1999**, *11*(1), 89.
(4) Wen, H. L.; Yen, F. S. *J. Cryst. Growth* **2000**, *208*, 696.
(5) Chang, P. L.; Yen, F. S.; Cheng, K. C.; Wen, H. L. *Nano Lett.* **2001**, *1*, 253.
(6) Cullity, B. D. *Elements of X-ray Diffraction*, 2nd ed.; Addison-Wesley: London, 1978.
(7) Klein, C.; Hurlbut, C. S., Jr. *Manual of Mineralogy*; John Wiley & Sons: New York, 1993.
(8) Hall, P. G.; Clark, N. S.; Maynard, S. C. P. *J. Phys. Chem.* **1995**, *99*, 5666.
(9) Cornell, R. M.; Schwertmann, U. *The Iron Oxides, Structure, Properties, Reactions, Occurrence and Uses*; VCH: Weinheim, 1996.
(10) Yang, J. M.; Tsuo, W. J.; Yen, F. S. *J. Solid State Chem.* **1999**, *145*, 50.
(11) Yang, J. M.; Tsou, E. J.; Yen, F. S. *J. Solid State Chem.* **2001**, *160*, 100.
(12) Schwertmann, U.; Taylor, R. M. *Clay Miner.* **1979**, *14*, 285.

NL010089M